fractal and fractional

Article

Modified FOPID Controller for Frequency Regulation of a Hybrid Interconnected System of Conventional and Renewable Energy Sources

Amil Daraz [1,2], Suheel Abdullah Malik [3], Abdul Basit [1,2], Sheraz Aslam [4] and Guoqiang Zhang [1,*]

1 School of Information Science and Engineering, NingboTech University, Ningbo 315100, China
2 College of Information Science and Electronic Engineering, Zhejiang University, Hangzhou 310027, China
3 Department of Electrical Engineering, FET, International Islamic University, Islamabad 44000, Pakistan
4 Department of Electrical Engineering, Computer Engineering and Informatics, Cyprus University of Technology, 3036 Limassol, Cyprus
* Correspondence: guoqiang_zhang@nbt.edu.cn

Abstract: In this article, a fractional-order proportional-integral-differential (FOPID) controller and its modified structure, called a MFOPID controller, are presented. To guarantee optimal system performance, the gains of the proposed FOPID and MFOPID controllers are well-tuned, employing the Jellyfish Search Optimizer (JSO), a novel and highly effective bioinspired metaheuristic approach. The proposed controllers are assessed in a hybrid system with two domains, where each domain contains a hybrid of conventional (gas, reheat, and hydro) and renewable generation sources (solar and wind). For a more realistic analysis, the presented system model includes practical limitations with nonlinear characteristics, such as governor dead zone/band (GDZ/GDB), boiler dynamics, generation rate limitation/constraint (GRL/GRC), system uncertainties, communication time delay (CTD), and load changes. The suggested methodology outperforms some newly developed heuristic techniques, including fitness-dependent optimizer (FDO), sine-cosine algorithm (SCA), and firefly algorithm (FA), for the interconnected power system (PS) of two regions with multiple generating units. Furthermore, the proposed MFOPID controller is compared with JSO-tuned PID/FOPID and PI controllers to ascertain its superiority. The results signify that the presented control method and its parametric optimization significantly outperforms the other control strategies with respect to minimum undershoot and peak overshoot, settling times, and ITSE in the system's dynamic response. The sensitivity analysis outcomes imply that the proposed JSO-MFOPID control method is very reliable and can effectively stabilize the load frequency and interconnection line in a multi-area network with interconnected PS.

Keywords: automatic generation control; fractional order PID controller; load frequency control; renewable energy source; jellyfish swarm algorithm; optimization techniques

Citation: Daraz, A.; Malik, S.A.; Basit, A.; Aslam, S.; Zhang, G. Modified FOPID Controller for Frequency Regulation of a Hybrid Interconnected System of Conventional and Renewable Energy Sources. *Fractal Fract.* **2023**, *7*, 89. https://doi.org/10.3390/fractalfract7010089

Academic Editor: Martin Čech

Received: 10 December 2022
Revised: 26 December 2022
Accepted: 6 January 2023
Published: 13 January 2023

1. Introduction

A power grid is a complex structure that integrates multiple systems with different load capacities. In today's large, interconnected power systems (IPS), load frequency management is critical to providing customers with excellent electrical performance and adequate system protection. The difference between the nominal frequencies and the actual frequency in interconnected areas is due to sudden load demands that result in an imbalance between generation and demand. Frequency differences induced by load changes can frequently result in a PS blackout. To avoid this scenario, automated generation control (AGC) employs a control approach capable of handling these abrupt load demands. AGC seeks to keep the system frequency and power flows between interconnected areas extremely close to their nominal levels [1–3].

To get a handle on the AGC problem, researchers have looked closely at regulating frequency to a certain level. A review of the relevant works reveals that a wide variety of work has been done in AGC by IPS. Simple conventional controllers including PID and PI are the most popular LFC regulators in the power sector because they are well-designed, inexpensive, and easy to implement [4,5]. In AGC analysis, the PID controller with various amended structures are predominantly employed in reference [6]. In [7], the authors used a modified PID controller for the LFC of two domains' IPS with multigeneration units, and demonstrated that it surpasses standard PI and PID controllers. The authors of [8] employed a doubly derived controller with integral parameters (IDD) for an AGC system and evaluated its efficiency with I/PI/PID controllers. The fundamental attempts of standard controllers do not achieve an excellent dynamic performance when there is a large variation in the magnitude of the step load. Some studies [9] also looked at AGCs that used a fuzzy logic controller (FLC) and an artificial neural network (ANN). To optimize system outputs more efficiently than conventional controllers, the FLC-based AGC controller count on the scaling agent, rule base assortment, membership function, and defuzzification process. However, FLC and ANN need significant computation time for database assessment and coaching.

From the literature assessment, most researchers have only addressed LFC problems related to traditional interconnected networks [10,11]. However, the architecture of the linked grid is continually changing as a result of changes in people's lifestyles, rising energy demand, industrialization, environmental concerns, and power grid modernization [12,13]. As a result, the earth is moving from a standard power supply to a hybrid power supply [14,15]. The diversity of renewable power generation and the obstruction of load demand are the main reasons for the fluctuation of frequency deviation, and a disturbance in one area of the control system also affects other areas of the dynamic control system. The oversaturation of non-traditional energy reserves and the inertia of the system are the main causes of system oscillations, which lead to changes in system frequency and interchangeable compound power [16,17]. On the other hand, exceeding the specified frequency limit leads to power failure or "blackout". It is obvious that the growing power grid will have problems with frequency management given the existence of renewable energy sources (RES) [18,19]. A modern control system is essential to providing the unavoidable power with an improved coherent frequency management that takes into account today's renewable resources.

The researchers used fractional order (FO) controllers, which are more frequently used for engineering problems due of their flexibility and increased level of freedom. In most circumstances, adding new pole types, such as hyper-damped poles, results in a greater need for tuning. As a result, the stability scale has been increased, enabling us to design a regulator that is more adaptable. Recently, LFC issues have been resolved using a tilt-integral-derivative (TID) controller, another representative of the FOC family. The TID controller has several benefits, including the flexibility with which closed-loop parameters can be changed, as well as its durability and improved disturbance rejection. Numerous research studies [20–22] have proposed the TID controller as a method to overcome LFC challenges. However, no attempt has yet been made in the literature to develop an improved form of the FOPID controller, known as MFOPID, for resolving interconnected conventional and renewable energy networks. As a result, the amended version of the FOPID controller with the JSO algorithm was successfully implemented for the LFC problem in this study.

Controller design alone is not sufficient to achieve optimal power system LFC. In LFC, optimization techniques are equally important for controller parameter selection. A variety of optimization techniques, such as the I- PD based Fitness Dependent Optimizer (FDO) [23], the Harries Hawks Optimizer (HHO) [24], the Artificial Electric Field Algorithm (AEFA) [25], the Path Finder Algorithm (FPA) [26], the FO controller optimized with Imperialist Competitive Algorithm (ICA) [27], the Grasshopper Optimization Algorithm (GOA) [28], the Salp Swarm Algorithm (SWA) [29], the Gorilla Troops Optimizer optimized with cascaded PI-FO PID controller [30], the PID and fuzzy PID controller adjusted with Modified Sine-Cosine Algorithm (MSCA) [31], the Gray Wolf Optimizer (GWO) [32], the Flower Pollination Algorithm (FPA) [33], the Marine Predator Algorithm (MPA) [34], the Improved Chaos Game Optimizer (ICGO) [35], and the optimized I- TD controller based on Water Cycle Algorithm (WCA) [36] have been used by intellectuals in the era of LFC. However, most of the aforementioned algorithms suffer from parametric compassion, premature convergence, and intricate computation. Therefore, a strong optimizer must be used to achieve the best performance. Hence, in this research study, a powerful bio-inspired metaheuristic computational approach term such as the Jellyfish search optimization (JSO) algorithm was developed. This algorithm was motivated by the way jellyfish hunt for food in the ocean. JSO differs from other swarming methods in that it converges quickly, is robust, uses fewer parameters, and avoids trapping in local minimums [37]. A broad scale of mathematical benchmark problems is employed to assess the effectiveness of the JS optimizer, as it is employed to resolve a variety of industrial problems. Solving the benchmark mathematical functions confirmed that the JS optimizer performed better than these algorithms. JSO has therefore been used to solve a diversity of engineering challenges [38–40]. According to the above discussion, the controller improvements resulted from the use of a modified FOPID controller, correct fractional computation, and a powerful optimizer for its parametric tuning. Therefore, a novel modified MFOPID controller and JSO are combined and proposed in this paper. To show the efficiency and reliability of the proposed JSO-based MFOPID controller, this combination (JSO: MFOPID) is utilized as a secondary mechanism to study the LFC in a hybrid power system based on an integral-of-time square error (ITSE) criterion.

Therefore, it is critical that a well-designed control unit be integrated into the power system. Also, proper constraints on the power system frequency and interconnection line must be maintained, and the system must be rebalanced as quickly as possible. In this study, a novel modified FOPID controller is developed as a trustworthy substitute method to improve the sustainability, reliability, and stability of a hybrid PS that includes conventional and RES such as solar and wind power. A novel metaheuristic technique called JSO is employed to fine-tune the gains of the proposed MFOPID controller. Below are some highlights of the inspiration, significance, and contributions of the current study:

- A new strong JSO-based bio-inspired approach is used to determine the parameters of the MFOPID controller to ensure optimal controller behavior, which is required to control the system's frequency and power variations.
- The realistic model was considered by integrating various nonlinearities such as GDZ, GRL, BD and CTD for a hybrid power system with conventional and RES such as photovoltaic and wind energy.
- A comparison of the performance of the MFOPID controller to that of FOPID, PI, and PID controllers to demonstrate its superiority.
- A demonstration of the efficacy of the JSO algorithm by comparing its performance with benchmark algorithms such as SCA, FA and FDO.
- The robustness of the suggested controller algorithm is evaluated using a series of test cases in which the load step perturbation (SLP) and system parameters are randomly altered.

2. Power System Model

Figure 1 shows a realistic model of a two-area hybrid interconnected system that comprises conventional and renewable energy sources with several nonlinearities, including BD, GRL, CTD, and GDZ, while conventional power generation systems include thermal power plants, hydroelectric power, a gas power unit, and RES including a wind and solar power unit. In addition, the physical limits of PS, including GDZ and GRC, are considered for nonlinearity and more realistic thermal unit analysis by using the GRC rate (0.0017 and 0.003 pu/s). In addition, the hydroelectric power plant generation rate limit is (0.06 p.u.) for decreasing rates and (0.045 pu/s) for increasing rates [41,42]. As shown in Equation

(1), a Fourier series is used to determine the transfer function (TF) for GDZ with a 0.50% margin [3].

$$GDZ/GDB = \frac{N_1 + N_2}{T_{sg} + 1} \tag{1}$$

where N_1 = 0.8 and $N_2 = \frac{-0.2}{\pi}$.

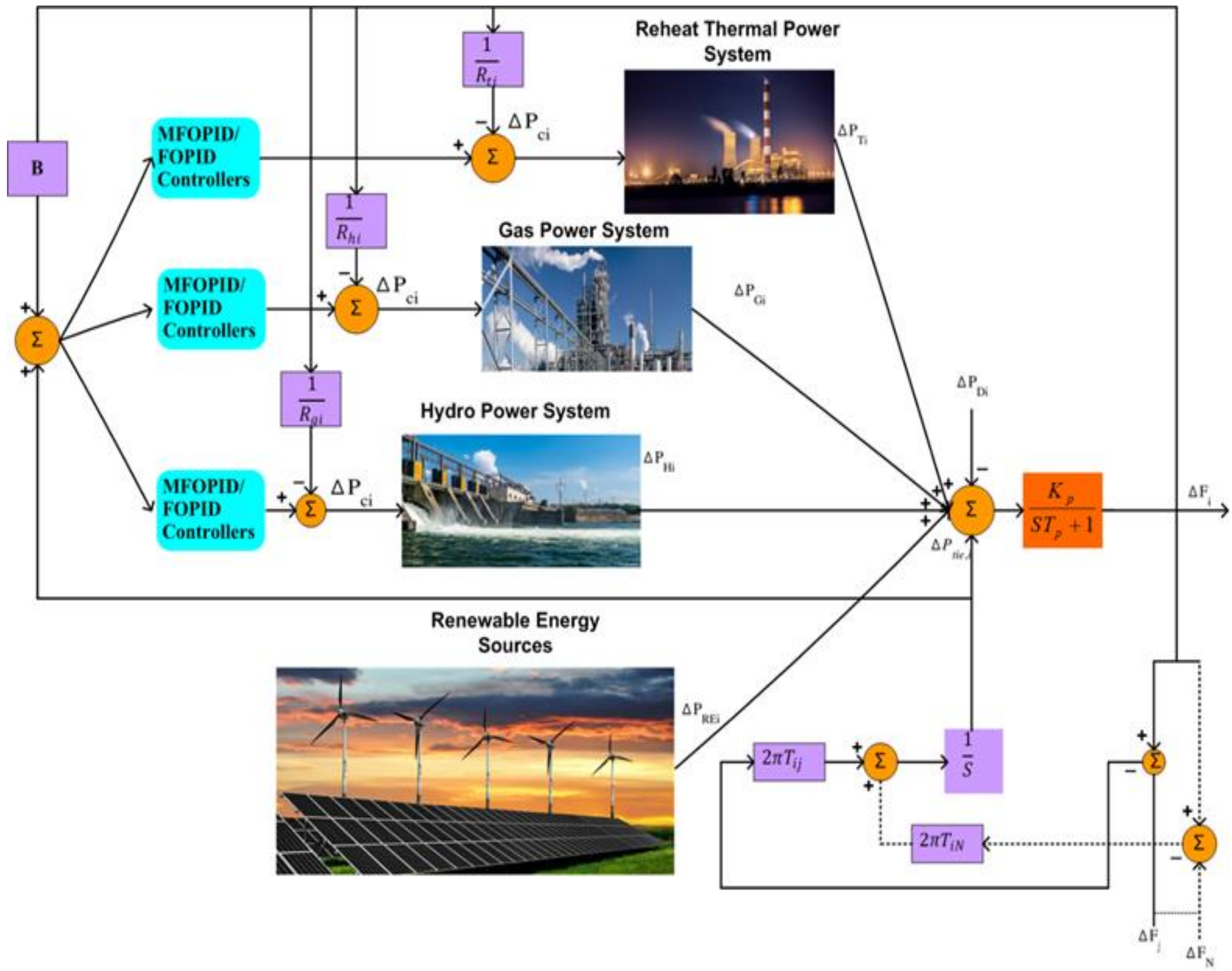

Figure 1. Schematic diagram of proposed power system.

Communication time delay (CTD) can affect controller execution and amplify system oscillations. Therefore, this work includes a simulation analysis that accounts for CTD in the controller fault domain (ACE) as well as other nonlinearities in the system. Figure 2 shows the TF model for the BD. This model is suitable for the analysis of both well-controlled coal-fired power plants and poorly controlled gas or oil-fired power plants. As soon as the boiler control system detects a change in steam flow rate or pressure variations, the corresponding controls are immediately activated [43]. This is how traditional steam power plants change their generation. The following equation illustrates the TF boiler dynamics model [44,45]:

$$T_{cpu}(s) = \frac{K_{1b}(1 + T_{1b}s)(1 + T_{rb}s)}{(1 + 0.1T_{rb}s)s} \tag{2}$$

$$T_f(s) = \frac{e^{-t_d(s)}}{Ts + 1} \tag{3}$$

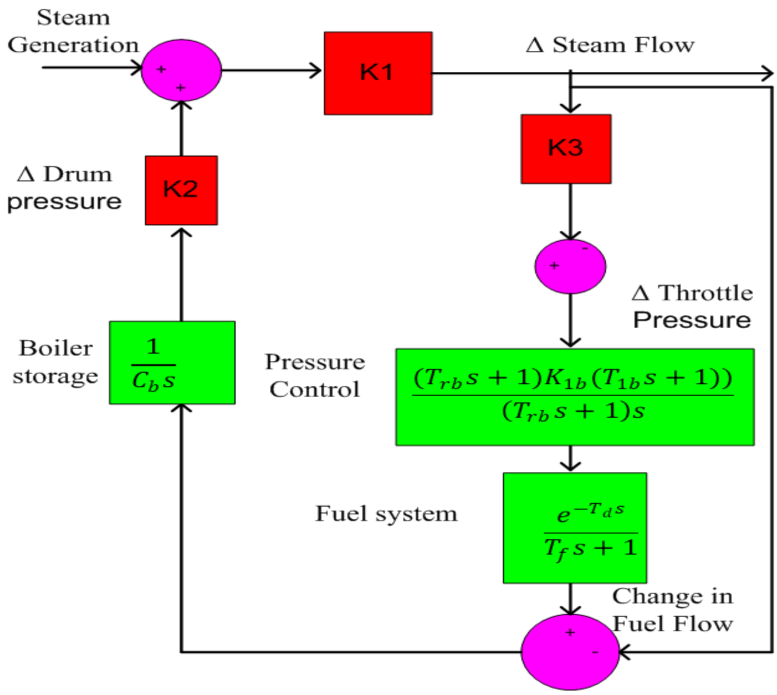

Figure 2. Schematic model of boiler dynamic.

Equations (4)–(6) represent the TF models of thermal, gas and hydro power plants, respectively [45].

$$G_{TR}(s) = \frac{1 + K_{re}T_{re}s}{(1 + T_{re}s)(1 + T_{gr}s)(1 + T_{gr}s)(1 + T_{tr}s)} \tag{4}$$

$$G_G(s) = \frac{a(I - T_{CR}s)(1 + Xs)}{(c + bs)(1 + T_{CD}s)(1 + Ys)(1 + T_{F}s)} \tag{5}$$

$$G_H(s) = \frac{(1 - T_w s)(1 - T_r s)}{\left(1 + T_{gh}s\right)(1 + 0.5T_w s)(1 + T_{rh}s)} \tag{6}$$

The Equations (4)–(6) correspondingly represent the TF models of thermal reheat, gas, and hydro power systems. Solar power plants use the sun's energy to produce both heat and electricity. Concentrating the sun's energy is critical to generating enough heat to run a power plant efficiently. Solar thermal concentration is used to create a thermodynamic heat-stream cycle [44,46,47]. Solar accumulators and the working fluid are critical components of an STPG system. Solar energy (air, water, or oil) is extracted using parabolic troughs that concentrate sunlight onto a circulating tube of working fluid. During the energy cycle, the working fluid is boiled in a boiler to produce high-pressure steam, which is then expanded in a turbogenerator to produce electricity. The STPG system can be linearized with distinct calculations, and the TF model for small signal analysis is specified as follows [47]:

$$G_s(s) = \frac{\Delta P_{STPG}}{\Delta P_{Solar}} = \frac{K_s}{1 + T_s s}\frac{K_T}{1 + T_T s} \tag{7}$$

K_T and K_S stand for the gain constants, T_T for the time constants of the steam turbine, and T_s for the time constants of the solar collector. As a mature source of renewable energy, wind energy has grown steadily in recent years, and its contribution to the power grid continues to increase. Although wind energy provides utility and environmental benefits, its irregular nature causes interconnection congestion and frequency fluctuations in the power grid. A rotor tilt control system is activated when wind speed fluctuates to ensure continuous wind turbine production. The WTPGs are analyzed and described by a first-order delay-based TF, as shown in Equation (8) [35].

$$G_{WTG}(s) = \frac{\Delta P_{WTPG}}{\Delta P_{wind}} = \frac{K_w}{1 + T_{WTG}s} \tag{8}$$

Here K_{WTG} is the wind power generation gain and T_{WTG} is the wind turbine time constant. The TF model for reheat thermal, gas, hydro and RES is shown in Figure 3a–d, respectively.

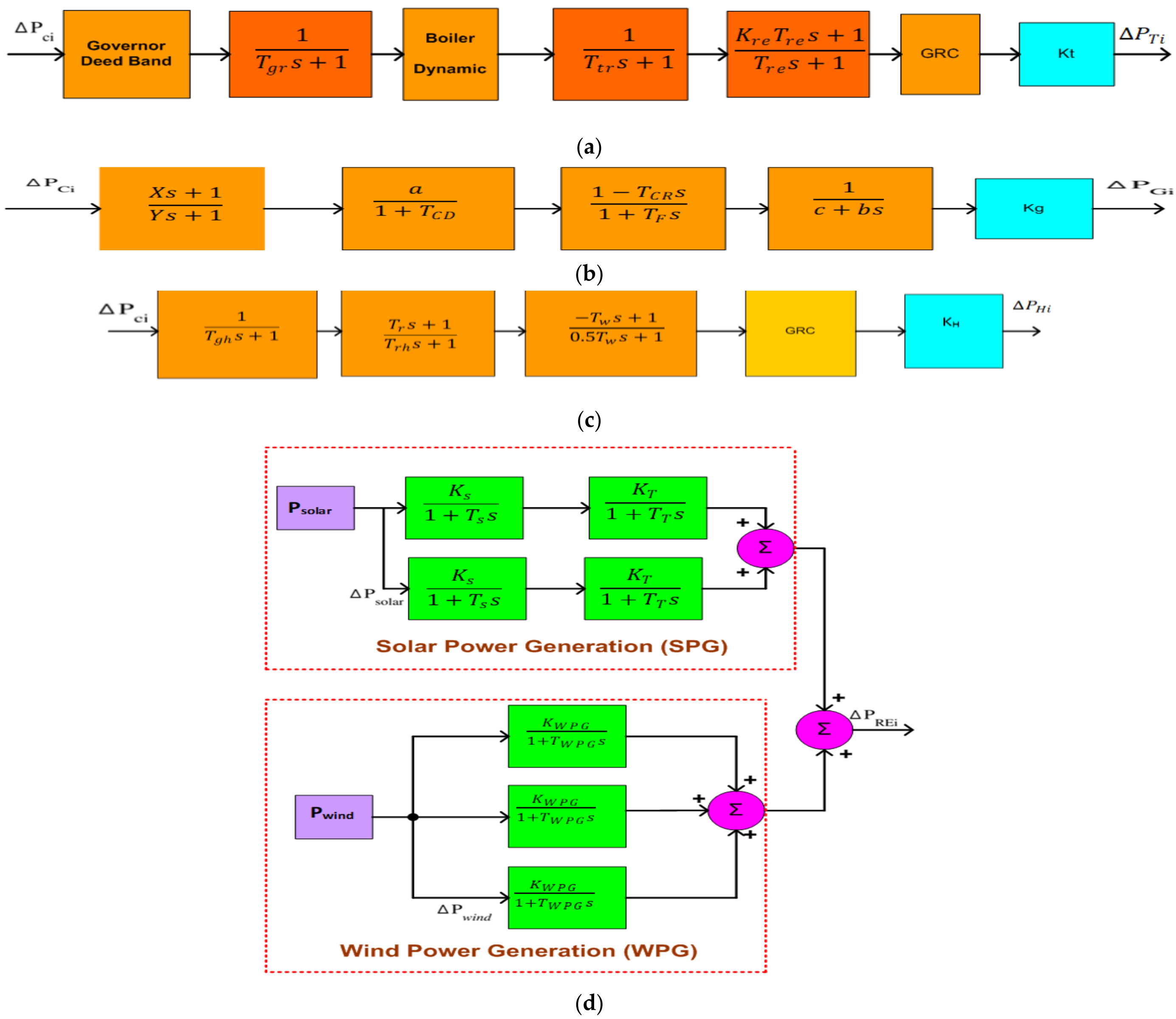

Figure 3. TF model for; (**a**) reheat thermal, (**b**) gas, (**c**) hydro, (**d**) RES.

3. Jellyfish Search Algorithm (JSO)

Chou and Truong developed and proposed the Jellyfish Search Optimizer (JSO), a revolutionary swarm-based optimization technique [37]. The algorithm is divided into the following sections.

3.1. Initialization of Population

To increase the variety of the starting inhabitants while retaining modesty, JSO employs a chaotic map term as the logistic map. As shown in Equation (9), it produces more distinct primary inhabitants than arbitrary collection and has a smaller chance of early convergence [37].

$$X_i + 1 = (1 - X_i)X_i\eta,\ 0 \leq X_i \leq 1 \tag{9}$$

Here X_i stands for the present spot of Jellyfish, X_{i+1} for the next spot and η represents constant value and is normally set to 4.

3.2. Following Ocean Current

The jellyfish are fascinated by the ocean current because it has a lot of food in it. By averaging the vectors from each individual jellyfish to the best-positioned jellyfish in the population, we can determine the route of the ocean stream. Equation (10) can be used to make a model of the ocean flow [37].

$$\overrightarrow{trend} = X^{\odot} - \beta \times rand(0,1) \times \mu \tag{10}$$

Here, $X^{\odot}$ denotes the best location of the jellyfish, β represents the distribution factor that is greater than 0, and μ represents the mean value of all jellyfish. Thus, Equations (11) and (12) provide the updated location of each jellyfish [37].

$$X_i(t+1) = X_i(t) + \overrightarrow{trend} \times rand(0,1) \tag{11}$$

$$X_i(t+1) = X_i(t) + rand(0,1) \times X^{\odot} - \beta \times rand(0,1) \times \mu \tag{12}$$

3.3. Jellyfish Swarm

When a school first forms, most jellyfish move in a passive manner. Over time, they become more active. Equation (13) gives the later updated position of each jellyfish [37].

$$X_i(t+1) = X_i(t) + (U_b - L_b) \times rand(0,1) \times \gamma \tag{13}$$

where $\gamma > 0$ is a coefficient of motion and L_b and U_b are the lower and upper limits of the quest space, respectively. The direction of movement and current place of a jellyfish are modeled by Equations (14)–(16). This organization is deemed to be a successful exploitation of the regional quest space [40].

$$\overrightarrow{Step} = \overrightarrow{Direction} \times rand(0,1) \tag{14}$$

$$\overrightarrow{Direction} = \begin{cases} X_k(t) - X_i(t); if\ f(X_i) \leq f(X_k) \\ X_i(t) - X_k(t); if\ f(X_i) < f(X_k) \end{cases} \tag{15}$$

Hence,

$$X_i(t+1) = \overrightarrow{Step} + X_i(t) \tag{16}$$

where f denotes the cost function at location X.

3.4. Time Control Mechanism

The time control process consists of a timing function $c(t)$ and a constant c_0 that allows the jellyfish to switch between following the ocean stream and migrating within the jellyfish swarm. The timing control function varies at random intervals from zero to one. The time-varying control function is given by Equation (17) [40].

$$c(t) = \left|(2 \times rand(0,1) - 1) \times (1 - \frac{t}{Max_{it}})\right| \tag{17}$$

where $c(t)$ is the timing function; c_0 is an initialized constant of 0.5; t is the timing given by the iteration number; and Max_{it} is the initialized parameter specifying the maximum number of iterations.

3.5. Boundary Conditions

Oceans exist in every corner of the earth. Since the planet is roughly spherical, a jellyfish swimming beyond the boundaries of the search area will eventually swim back to the opposite boundary. Equation (18) illustrates this process of re-entry [40].

$$X'_{i,j} = \begin{cases} X_{i,j} - U_{b,j} + L_{b,j}; & if\ X_{i,j} > U_{b,j} \\ X_{i,j} - L_{b,j} + U_{b,j}; & if\ X_{i,j} < U_{b,j} \end{cases} \tag{18}$$

where $L_{b,j}$ and $U_{b,j}$ are the lower and upper limits in the jth magnitude of the quest space, $X_{i,j}$ is the position of the ith jellyfish in the jth dimension, and $X'_{i,j}$ is the updated position after applying the boundary conditions. The schematic flowchart for JSO is shown in Figure 4.

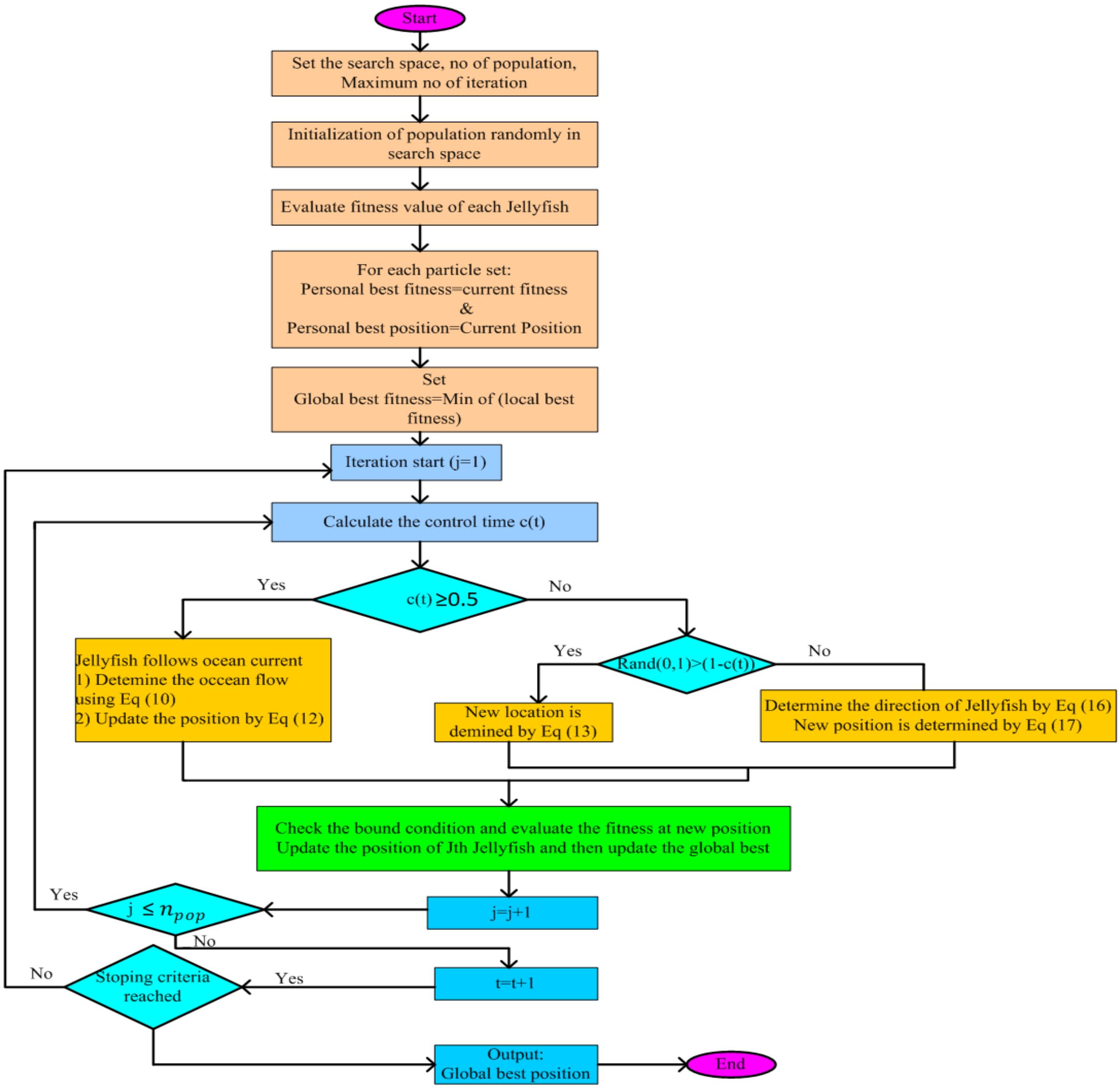

Figure 4. The Schematic flow chart for JSO.

4. Controller Structure and Fitness Function

Various AGC regulators have been developed and employed in the previous studies. However, in recent years, much consideration has been paid to fractional order controllers compared to conventional controllers due to their higher noise rejection ratio, lower noise impact, and shorter computation time [4,47–49]. In this portion, a MFOPID controller is developed and employed for AGC problems in conventional and renewable energy sources. Figures 5 and 6 shows the configuration of FOPID and MFOPID controllers respectively, which include five parameters: Integral term (K_i), proportional term (K_p), derivative term (K_d), fractional derivative order (μ) and fractional integrator order (λ). In the FOPID controller, all of the gains are feedforwarded, while in the MFOPID controller, the integral term (K_i) is feedforward with the integrator order (λ) and the other parameters are feedback. Equations (19) and (20) give the output of the FOPID and MFOPID controller, respectively, in the form of a differential equation.

$$u(t) = e(t)K_p + e(t)D^{-\lambda}K_i + e(t)D^{\mu}K_d \tag{19}$$

$$u(t) = e(t)D^{-\lambda}K_i - y(t)\left[K_p + D^{\mu}K_d\right] \tag{20}$$

where $u(t)$ is the control signal, $e(t)$ is the error term, and $y(t)$ is the system productivity. An instantaneous step shift in the output signal $U(s)$ is caused by a step change in the setpoint of the FOPID controller. This sudden increase in the output controller is called a "proportional kick" or "derivative kick" and rapidly changes the actuator control signal. The updated structure of the FOPID controller was introduced to address these shortcomings. The integral gain (Ki) in this structure responds to the error signal $E(s)$. The derivative and proportional gains are unaffected by a sudden change in the setpoint input, since these two-terms act on the process output ($Y(s)$) [44]. By utilizing a plant $G(s)$ and the corresponding FOPID and MFOPID controllers, we obtain Equations (21) and (22), which represent the corresponding transfer functions (TFs) of the control loops.

$$\frac{Y(s)}{R(s)} = \frac{[S^{\lambda}K_p + K_d S^{\lambda} S^{\mu} + K_i]G_p(s)}{S^{\lambda} + [S^{\lambda}K_p + K_d S^{\lambda} S^{\mu} + K_i]G_p(s)} \tag{21}$$

$$\frac{Y(s)}{R(s)} = \frac{G_p(s)K_i}{S^{\lambda} + S^{\lambda}K_p + G_p(s)K_i + K_d S^{\lambda} S^{\mu}} \tag{22}$$

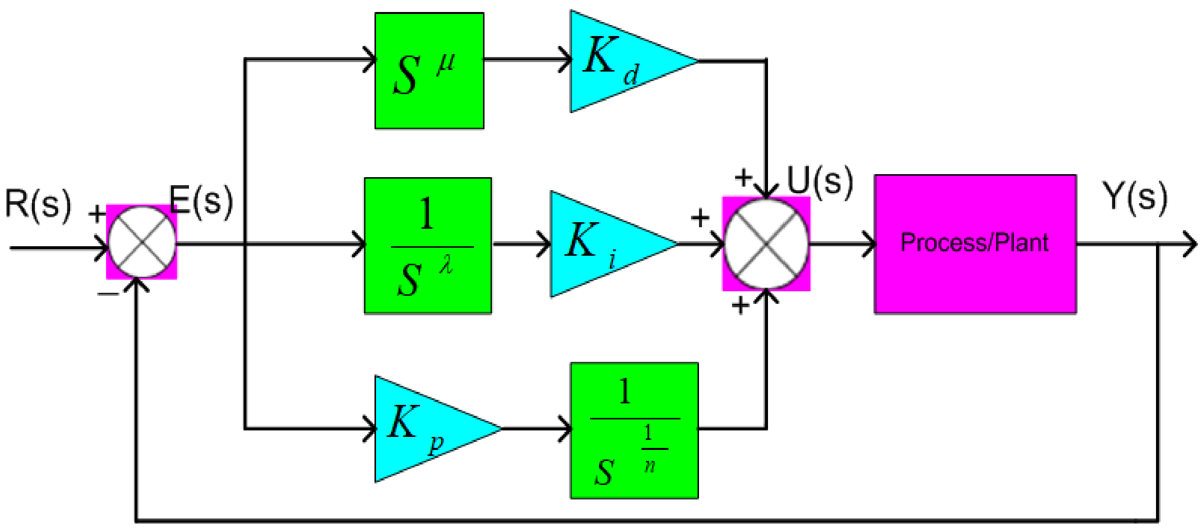

Figure 5. Structure of FOPID controller.

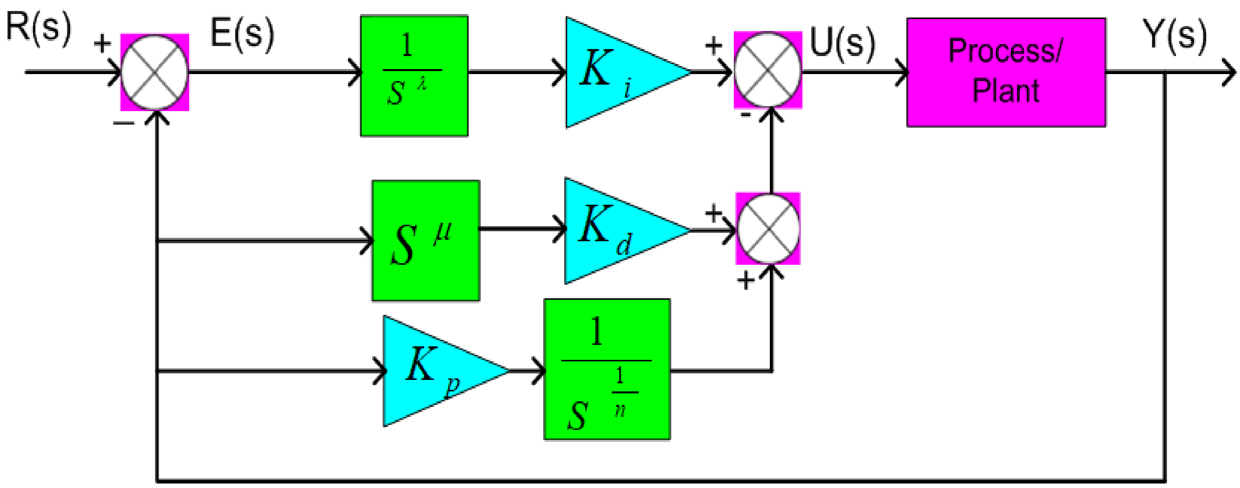

Figure 6. Structure of MFOPID controller.

Equation (21) shows that the FOPID controller has two zeros and that it is difficult to change the response of the system when this is the case. Its effect is either a more extreme overshoot or a faster rise to the peak value. The proposed modified FOPID controller, also called a MFOPID controller, overcomes these effects of zeros according to Equation (22) and improves the system response by placing the K_p and K_d gains of the FOPID controller on the feedback route in lieu of the forward direction. As a result, the system response with the MFOPID controller is better than the system response with the FOPID controller, as shown in the Results and Discussion section. (ITSE) refs. [3,23,44,46] are employed as a cost function to resolve the LFC problem of interconnected hybrid PS using the JSO approach. The expression for ITSE can be written as follows [3,23].

$$\text{ITSE} = J = \int_0^t \left[\left| \Delta \text{F}_1^2 + \Delta \text{F}_2^2 + \Delta \text{P}_{tie}^2 \right| \right] t dt \tag{23}$$

Variables in the design have inherent constraints and restrictions. Therefore, the provided imperatives should not be ignored while attempting to identify the optimal solution. Considering this, the current optimization problem contains the following design constraints:

Minimize ITSE

Subject to:

$$\begin{array}{c} K_p^{Min} \leq K_p \leq K_p^{Max} \\ K_d^{Min} \leq K_d \leq K_d^{Max} \\ K_i^{Min} \leq K_i \leq K_i^{Max} \\ \lambda^{Min} \leq \lambda \leq \lambda^{Max} \\ \mu^{Min} \leq \mu \leq \mu^{Max} \end{array} \tag{24}$$

In Equation (24), Min and Max represent the minimum and maximum controllable variable ranges for the MFOPID controller. This study also selects the limitations for differentiator and integrator coefficient (λ, μ = 0 to 1), proportional, integral, and derivative gain (K_p, K_i, K_d = −2 to 2) to obtain optimal controller design variables on a broad scale. Ultimately, the optimal solution for MFOPID controller design variables is identified within the specified constraints for the smallest ITSE values by investigating the benefits of the productive searching characteristics of JSO.

5. Implementation, Results and Discussion

The schematic model depicted in Figure 1 is constructed in Simulink/Matlab utilizing the parametric values from Appendix A. The ITSE benchmarks are employed as a cost function to adjust the parameters of the suggested MFOPID controller. The values of the JSO parameters were selected from Appendix B for optimizing the controller gains. For each algorithm, the optimization process was repeated 20 times, and the best values from the 20 iterations were selected as the final gains of the controller. Table 1 shows the best results for interconnected regions with six generating units including conventional and RES for different circumstances. The results of the proposed methodology are comparable to other approaches such as the SCA, FA and FDO-based MFOPID methods. Figure 7 shows an ITSE-based convergence profile of the various algorithms. For the AGC problem of hybrid power systems with conventional and renewable energy supply, two cases were studied. In the first scenario, the proposed JSO method is associated with other optimal methods such as SCA, FA, and FDO. In the next scenario, the execution of the suggested unique controller has been compared with the achievement of different traditional controllers such as PID, PI and FOPID. In addition, a robustness test is accomplished to demonstrate the practicality of the suggested controller.

Table 1. Optimal gains of the suggested controller considering case 1 and case 2.

Controller Gains	Case 1				Case 2			
	MFOPID (FA)	MFOPID (SCA)	MFOPID (FDO)	MFOPID (JSO)	MFOPID (JSO)	FOPID (JSO)	PID (JSO)	PI (JSO)
K_{p1}	1.543	1.903	0.998	1.340	1.101	0.789	1.234	1.230
K_{i1}	0.910	1.234	1.010	1.543	0.002	1.020	1.987	1.110
K_{d1}	1.023	1.678	1.900	0.220	0.010	0.789	0.303	
λ_1	0.789	0.006	0.100	0.223	0.090	0.765		
μ_1	0.675	0.124	0.165	0.972	0.002	0.013		
K_{P2}	0.032	1.011	1.810	0.011	1.009	0.303	0.300	1.009
K_{i2}	0.024	1.304	1.020	0.991	1.199	1.109	0.340	1.199
K_{d2}	0.100	1.008	1.200	0.910	−1.560	1.001	1.090	
λ_2	0.165	0.165	0.010	0.165	0.059	0.090		
μ_2	0.003	0.003	0.090	0.013	0.564	0.002		

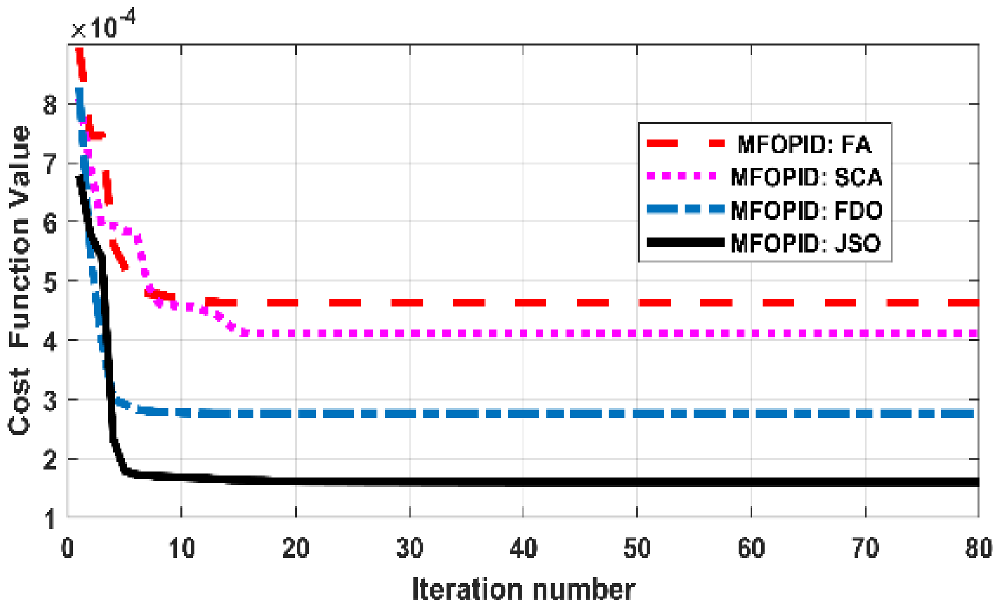

Figure 7. Convergence profile for various algorithms.

5.1. Case-1 (Comparison in Terms of Algorithm)

In this scenario, the dominancy of the proposed JSO technique is evaluated by comparing the results with other optimization strategies such as SCA, FA and FDO. Figure 8a–c shows the system response using the proposed methods for a load step of 1% in region

1. The JSO-based optimization technique swiftly controlled the fluctuation for frequency variation in region-1 (ΔF_1), region-2 (ΔF_2), and interconnected region power (ΔP_{tie}), as shown in Figure 8a–c. Table 2 provides a detailed comparison of the results for the different algorithms in terms of settling time (T_s), overshoot (O_{sh}), and undershoot (U_{sh}) for ΔF_1, ΔF_2, and ΔP_{tie} variation. According to Figure 8a–c, the MFOPID controller optimized with the JSO algorithm has approximately the identical peak overshoot as the MFOPID tuned with the FDO approaches, but an 19.73% improved settling time for the variation of region-1 and 23.98% for the variation of region-2. Similarly, compared to the MFOPID controller tuned with SCA, the MFOPID controller adjusted with JSO enhance the time settling by (51.36%, 17.96%, and 1.09%) and effectively reduced overshoot by (98.08%, 76.11%, and 73.14%) for range-1, range-2, and the change in connected power, respectively. Table 2 shows that compared with the controller based on hDE- PS (MID), the tuned MFOPID controller based on JSO provides a significant improvement of 81.56%, 36.98%, and 33.98% for both (ΔF_1), (ΔF_2),and (ΔP_{tie}), while effectively reducing the peak overshoot by 98.45%, 79.33%, and 41.80% and the undershoot by 7.36%, 65.01%, and 76.01% for region-1, region-2, and the variation of tie-line power, respectively. Similarly, compared with TID controller tuned with the hybrid TLBO based PS algorithm [22], the JSO-based MFOPID controller improves the T_s by 63.81%, 06.67%, and 09.55% for the load frequency of region-1, region-2, and the variation of power in the interconnected grid, respectively. According to Figure 7, the JSO method converges quickly using the ITSE conditions and reaches a value of (ITSE =0.000171) compared to SCA with ITSE = 0.000421, FDO(ITSE = 0.000521) and FA (ITSE = 0.000301). The whole comparison in terms of percentage improvement considering case-1 for (ΔF_1), (ΔF_2), and (ΔP_{tie}) variation is shown in Figure 9.

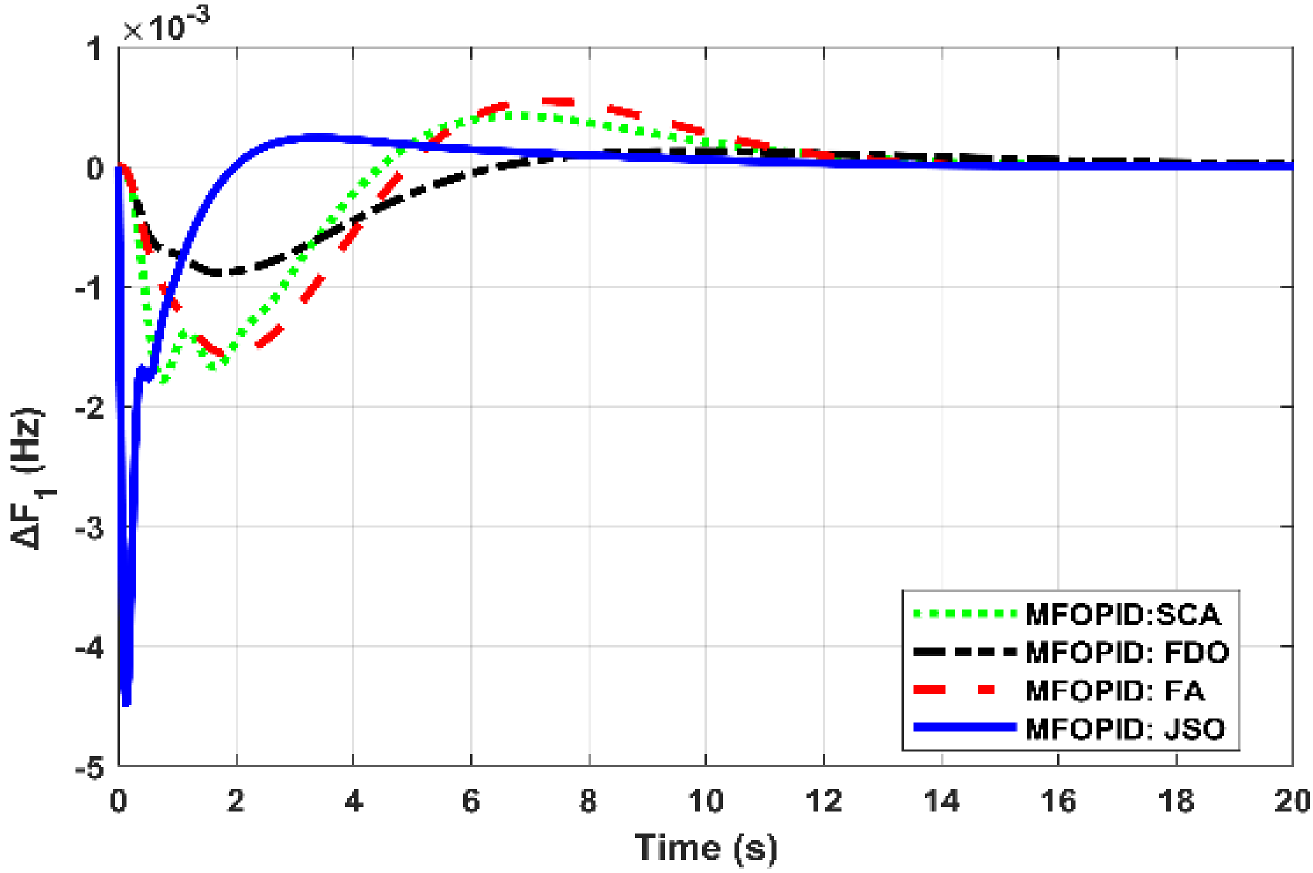

(**a**)

Figure 8. *Cont.*

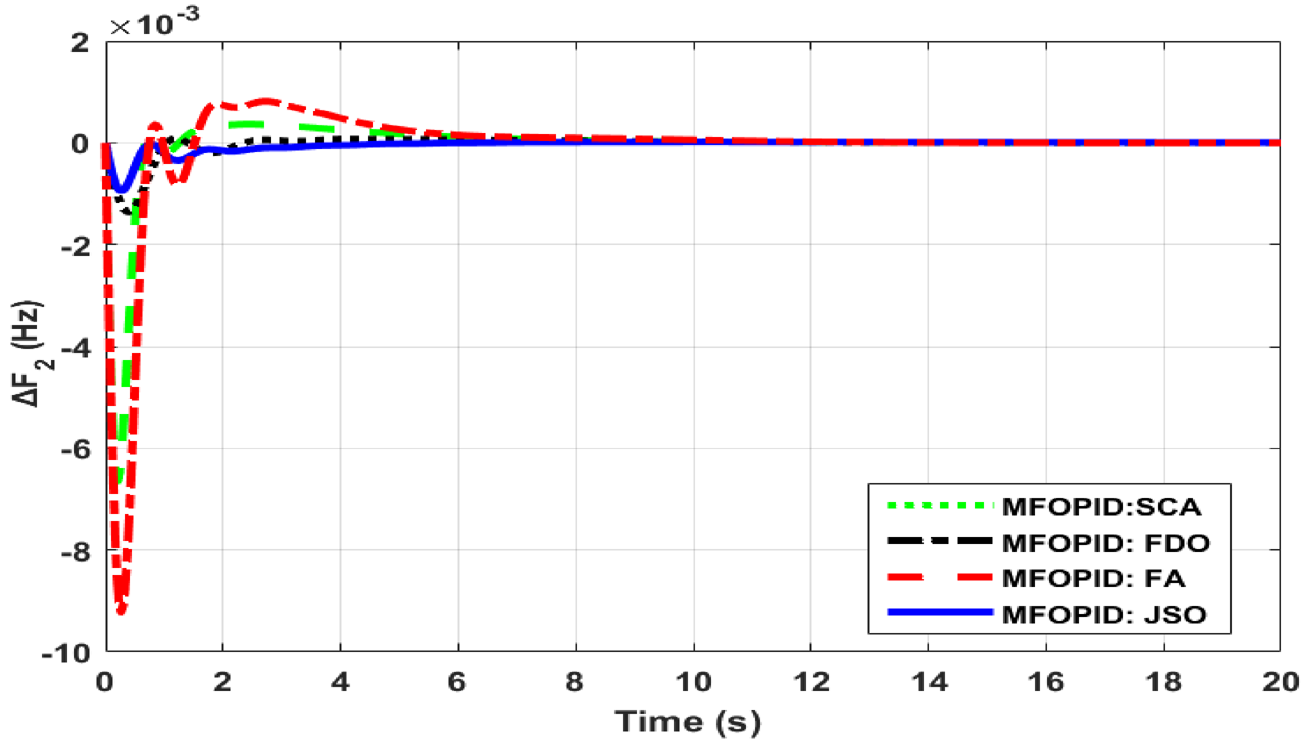

(**b**)

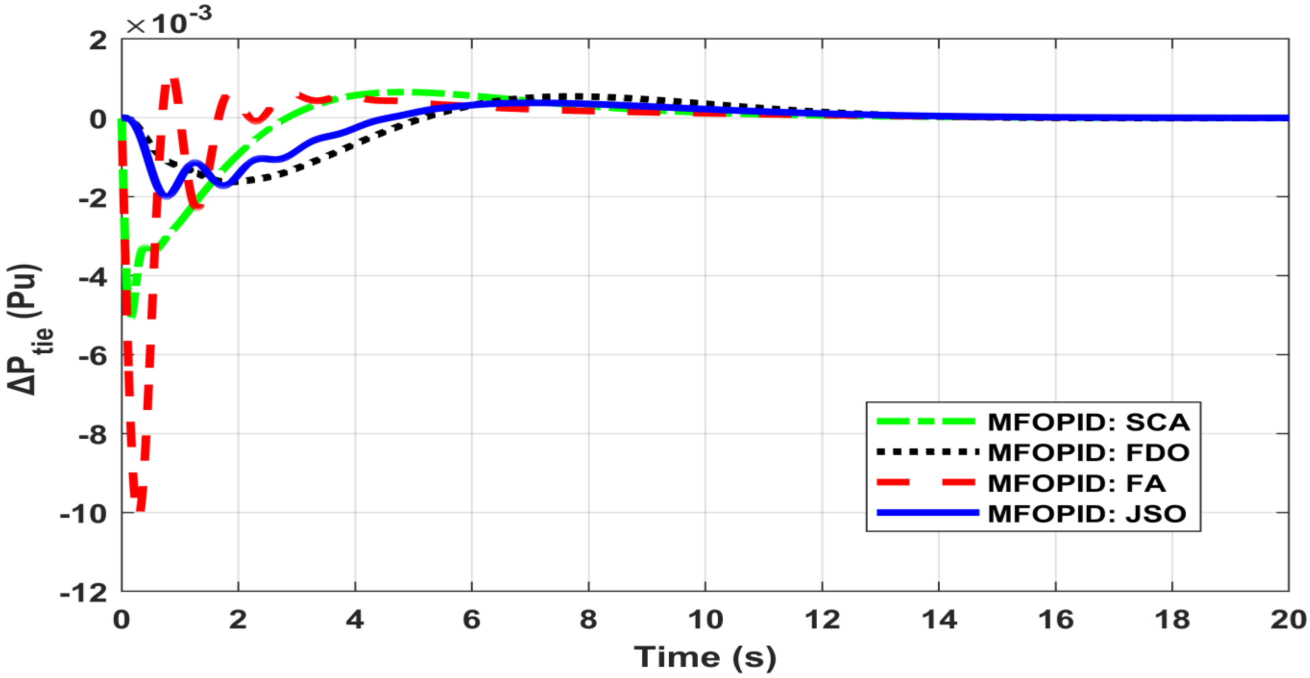

(**c**)

Figure 8. Output response of the PS considering case −1 for (**a**) ΔF_1; (**b**) ΔF_2; (**c**) ΔP_{ite}.

Table 2. Numerical results for a hybrid power system considering case-1.

Controller with Algorithms	Settling Time (T_s)			Overshoot (Osh)			Undershoot (Ush)		
	ΔF_1	ΔF_2	ΔP_{tie}	ΔF_1	ΔF_2	ΔP_{tie}	ΔF_1	ΔF_2	ΔP_{tie}
MFOPID: JSO	**13.1**	**4.42**	**9.81**	0.000240	**0.000017**	**0.000378**	−0.00448	**−0.00094**	−0.00199
MFOPID: FDO	15.9	5.02	9.83	0.000126	0.000082	0.000651	**−0.00088**	−0.00135	−0.00507
MFOPID: SCA	14.8	6.53	12.7	0.000424	0.000363	0.000542	−0.00178	−0.00664	**−0.00162**
MFOPID: FA	14.7	8.43	9.99	0.000548	0.000813	0.001236	−0.00156	−0.00922	−0.01012
hTLBO-PS: TID [22]	13.75	9.53	10.36	0.070400	0.007222	0.003500	−0.24010	−0.18888	−0.06330
hDE-PS: MID [43]	18.09	19.07	12.69	0.001700	0.000800	0.000600	−0.01500	−0.00100	−0.00800

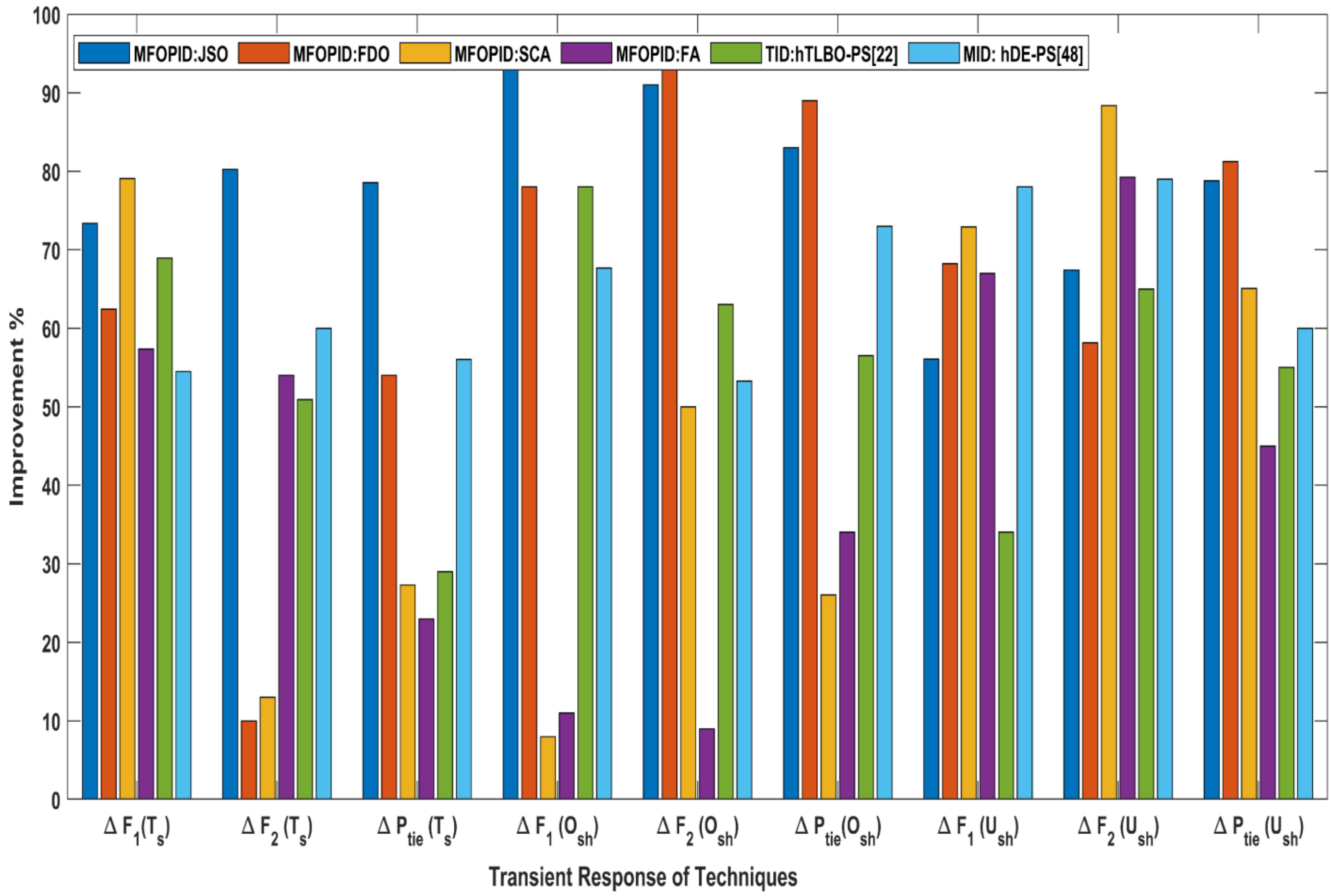

Figure 9. Bar graph of percentage improvement considering case 1.

5.2. Case-2 (Comparison in Terms of Controller)

In this scenario, the effectiveness of a MFOPID controller adjusted with the JSO approach was compared with the performance of FO-PID, PID, and PI controllers adapted with the same technique. Figure 10a–c and Table 3 show the results obtained with the mentioned schemes. Table 3 reveals that the MFOPID controller with the JSO-tuned approach outperforms the FOPID controller tuned with JSO techniques in terms of settling time (3.11%, 21.34%, and 32.56%) and overshoot (73.12%, 55.01%, and 89.16%) for region-1, region-2, and interlink power variation, respectively. Compared to a PID controller optimized with similar algorithms, the MFOPID controller improved the settling time by (54.11%, 17.34% and 26.10%), effectively reducing the peak overshoot by (56.30%, 79.67% and 90.22%), for region-1, region-2, and the interconnection power variation, respectively. It can be also observed from Table 3 that the FOPID controller also shows good performance in terms of undershoot as compared to PID and the PI controller. Thus, we can conclude that our proposed controller outperforms the PID and PI controllers optimized with a similar algorithm, namely JSO, in terms of U_{sh}, T_s, and O_{sh}. The whole comparison in terms of percentage improvement considering case-2 for (ΔF_1), (ΔF_2), and (ΔP_{tie}) variation is shown in Figure 11.

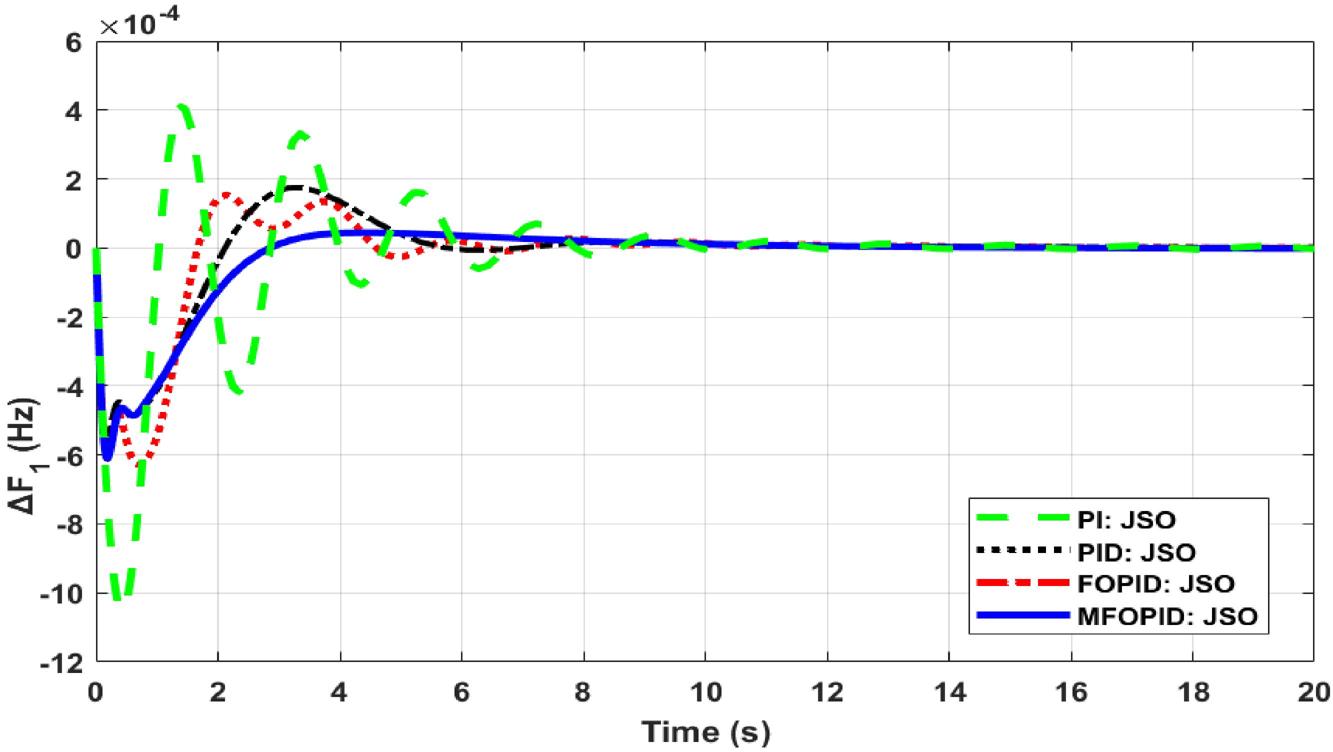

(**a**)

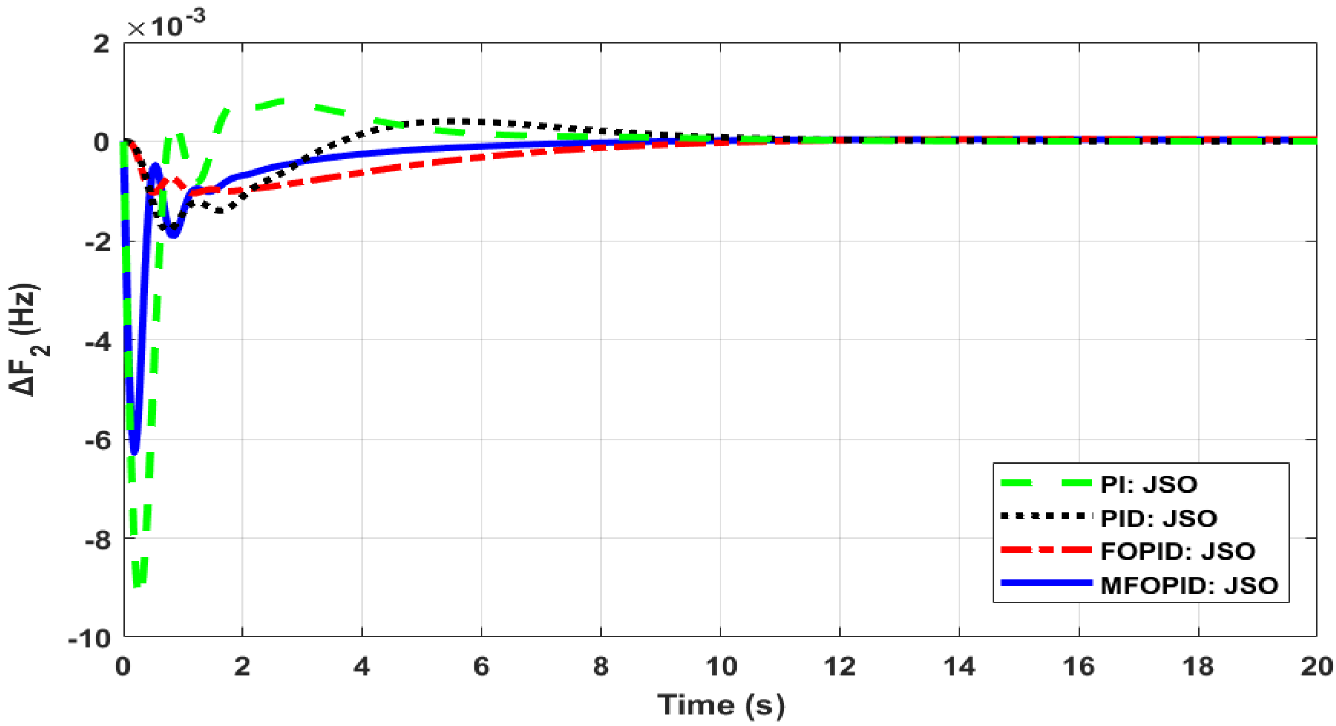

(**b**)

Figure 10. *Cont.*

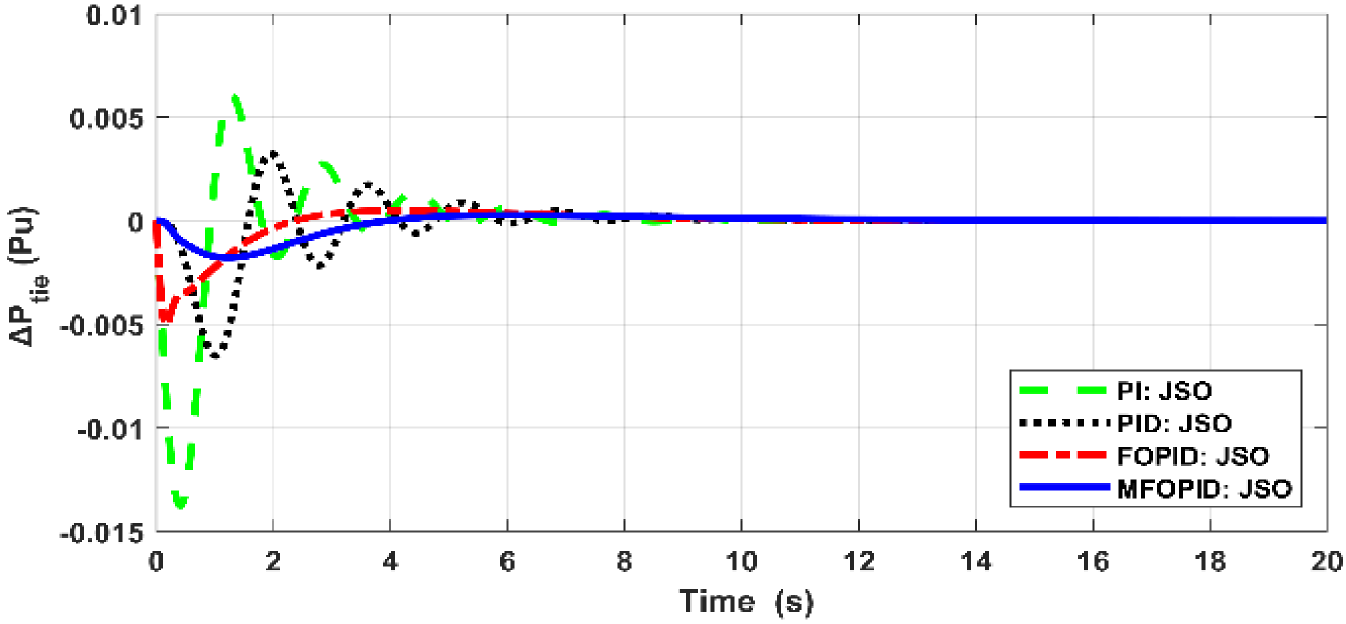

(c)

Figure 10. Output response of the PS considering case−2 for (**a**) ΔF_1; (**b**) ΔF_2; (**c**) ΔP_{ite}.

Table 3. Numerical results for hybrid power system considering case-2.

Techniques	Settling Time (T_s)			Overshoot (Osh)			Undershoot (Ush)		
	ΔF_1	ΔF_2	ΔP_{tie}	ΔF_1	ΔF_2	ΔP_{tie}	ΔF_1	ΔF_2	ΔP_{tie}
MFOPID: JSO	**10.9**	**6.23**	**8.23**	**0.000044**	**0.000041**	**0.000272**	−0.00061	−0.00628	**−0.00178**
FOPID: JSO	11.1	7.93	8.46	0.000174	0.000048	0.000509	**−0.00056**	**−0.00104**	−0.00500
PID: JSO	11.0	8.61	9.02	0.000153	0.000406	0.003254	−0.00062	−0.00179	−0.00651
PI: JSO	12.2	10.9	10.4	0.000409	0.000813	0.006035	−0.00105	−0.00922	−0.01376

5.3. Sensitivity Analysis

A sensitivity analysis was undertaken to study the unpredictability of the dynamic behavior of a power system under nominal conditions with respect to a specific change in a small part of the fundamental parameters of the system. This analysis aimed to study the robustness of the controller performance by changing the system parameters. In this study, the synchronization coefficient (T_{12}), droop constant (R) the governor time constant (T_g), and the reheat thermal constant (T_{rh}) were varied in a range of ±40% to determine the sensitivity of several system parameters at nominal values. Figure 12a–c shows the outcome attained by adjusting the system settings in the range of ±40%. Table 4 compares several parameters in terms of Ts, U_{sh} and O_{sh} at a deviation of ±40% from their nominal values. From Table 4, it can be seen that the system response for several parameters is almost identical to the nominal values. This shows that the intended JSO-based MFOPD controller delivers robust execution over a scale of ±40% of the PS parameters. Moreover, the optimal values of the suggested controller do not need to be retuned for a wide range of parameters at nominal capacity with nominal parameters.

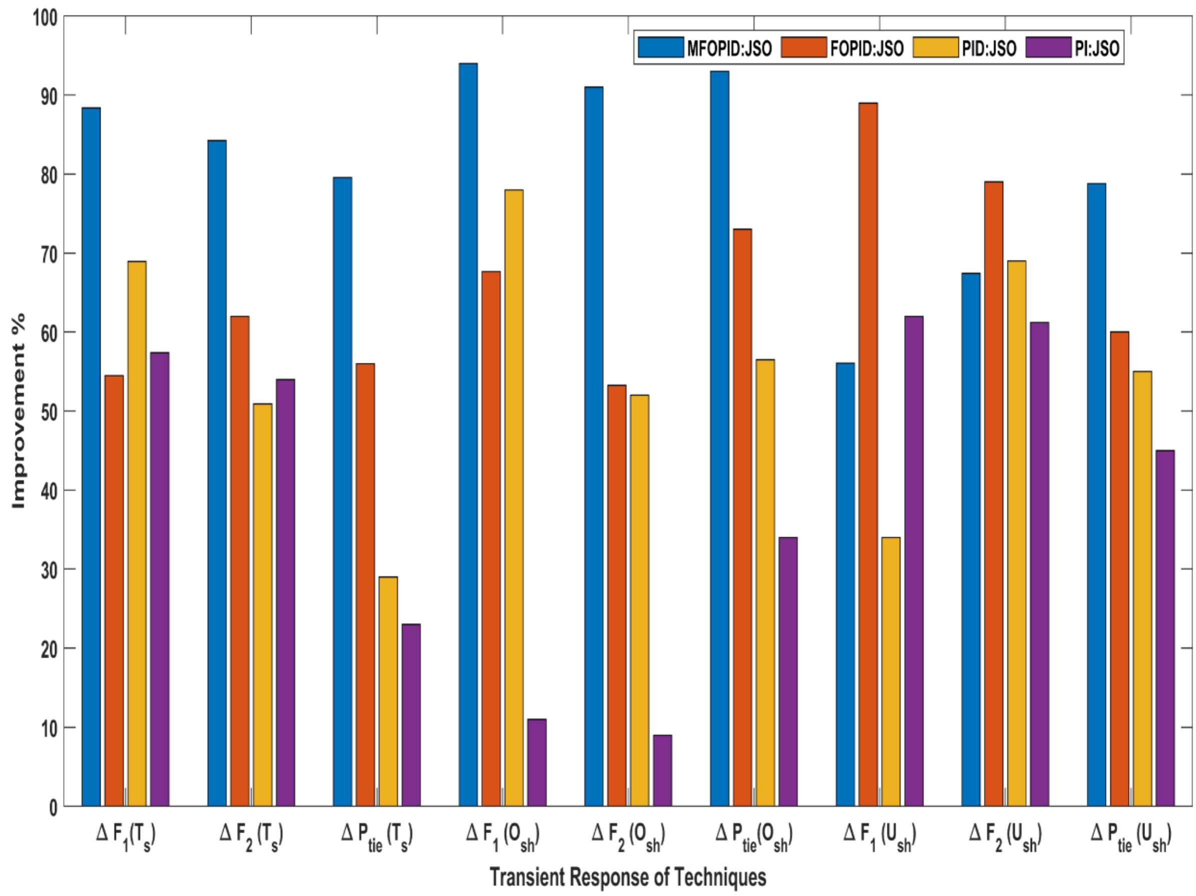

Figure 11. Bar graph of percentage improvement considering case 2.

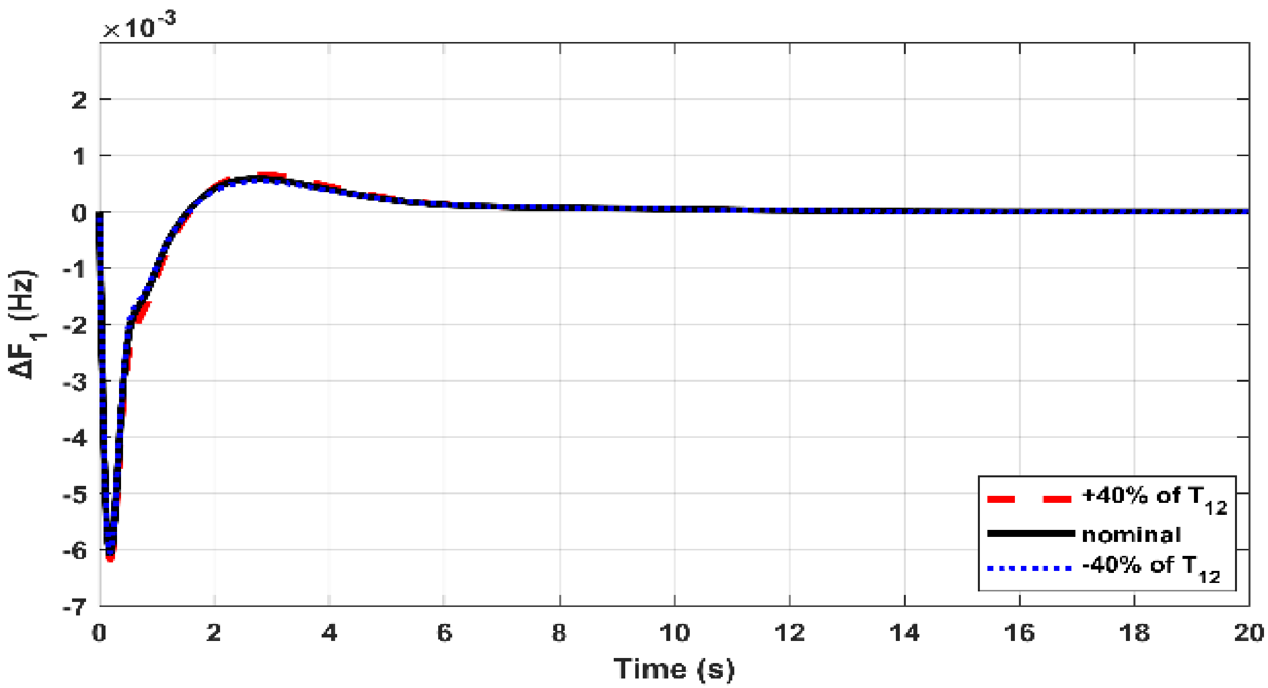

(a)

Figure 12. *Cont.*

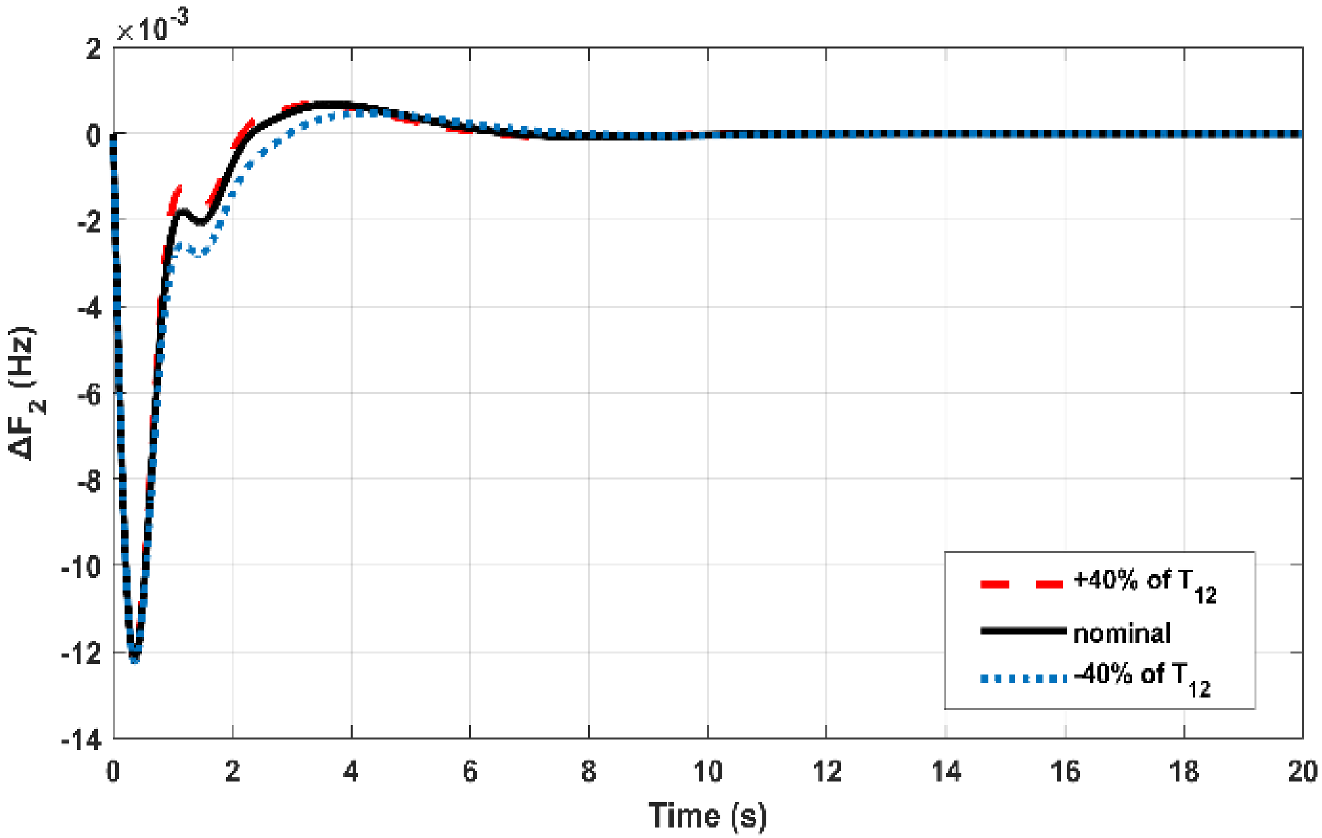

(**b**)

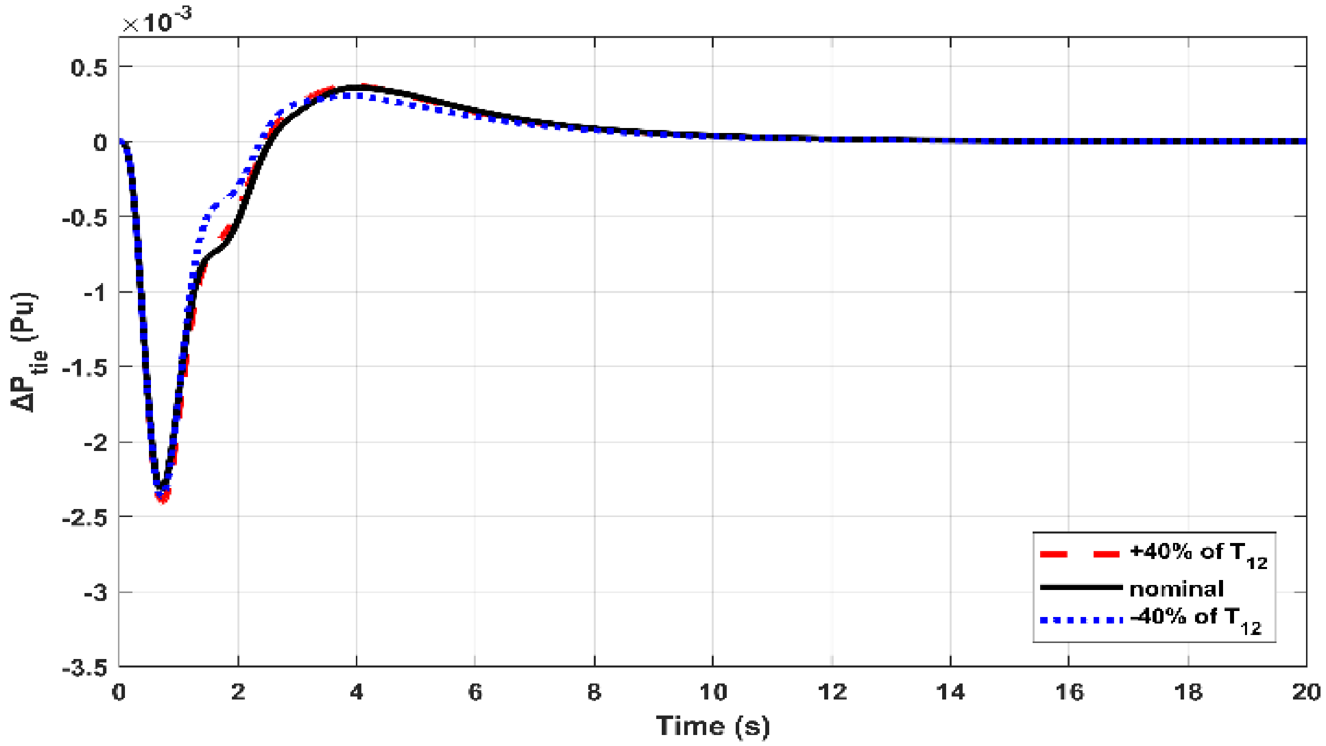

(**c**)

Figure 12. Robustness performance of proposed MFOPID controller for: (**a**) ΔF_1; (**b**) ΔF_2; (**c**) ΔP_{ite}.

Table 4. Sensitivity analysis of the proposed controller for hybrid PS.

Parameters	% Variation	Settling Time (T_s)			Overshoot (Osh)			Undershoot (Ush)		
		ΔF_1	ΔF_2	ΔP_{tie}	ΔF_1	ΔF_2	ΔP_{tie}	ΔF_1	ΔF_2	ΔP_{tie}
T_g	+40	6.38	6.78	12.72	0.00068	0.00064	0.000323	−0.00240	−0.00610	−0.00315
	−40	8.01	7.90	12.73	0.00047	0.00054	0.000276	−0.00236	−0.00600	−0.00313
R	+40	6.38	6.74	13.01	0.00037	0.00094	0.000296	−0.00713	−0.00693	−0.00489
	−40	8.03	7.91	13.03	0.00030	0.00098	0.000289	−0.00913	−0.00678	−0.00482
Trh	+40	6.10	6.14	12.80	0.00014	0.00083	0.000310	−0.00780	−0.00731	−0.00361
	−40	7.80	8.10	12.79	0.00017	0.00075	0.000311	−0.00740	−0.00725	−0.00361
T_{12}	+40	6.09	6.17	13.10	0.00032	0.00063	0.000315	−0.00830	−0.00623	−0.00251
	−40	7.82	8.10	13.08	0.00031	0.00061	0.000316	−0.00840	−0.00618	−0.00257

6. Conclusions and Future Direction

The MFOPID controller was built and developed in this work for the AGC of two domains, hybrid conventional and renewable energy sources, with the addition of various nonlinearities such as GDZ, BD, CTD and GRL. The bioinspired metaheuristic algorithm Jellyfish Optimizer Search (JSO) was used to optimize the settings of the proposed controller. The simulation results show that the JSO based tuned MFOPID controller provides significance of 81.56%, 36.98% and 33.98% for both regions and link power while successfully reducing peak overshoot by 98.45%, 79.33% and 41.80% and undershoot by 7.36%, 65.01% and 76.01% for region-1, region-2 and link power variation respectively. Similarly, compared with the (TID: hTLBO-PS), the JSO based MFOPID controller improves the Ts by 63.81%, 06.67% and 09.55% for the load frequency of region-1, region-2, and interconnect power, respectively. Finally, the resilience of the MFOPID controller is investigated by deviating the system parameters from the minimal values. The findings show that the gains of the proposed controller are not reset when the system parameters or load conditions change. The effectiveness of the JSO-based MFOPID controller reveals that the controller is capable of efficiently solving AGC problems in hybrid power systems with sustained oscillations. In the future, the proposed control configuration may be applied for various other energy sources in a deregulated environment.

Author Contributions: Conceptualization, S.A.M. and G.Z.; methodology, A.D.; software, A.D., A.B.; validation, S.A.M., S.A. and A.B.; formal analysis, S.A.M. and A.B.; investigation, G.Z.; resources, G.Z.; data curation, S.A.; writing—original draft preparation, A.D., A.B.; writing—review and editing, S.A.M. and G.Z.; visualization, S.A. and A.B.; supervision, G.Z.; project administration, S.A.M., and G.Z.; funding acquisition. All authors have read and agreed to the published version of the manuscript.

Funding: This research work was funded by "Young talent Sub-project of Ningbo Yongjiang Talent Introduction Programme" under grant number 20100859001.

Institutional Review Board Statement: Not applicable.

Informed Consent Statement: Not applicable.

Data Availability Statement: No new data were analyzed or generated in this study. Data sharing is not appropriate to this manuscript.

Conflicts of Interest: The authors declare no conflict of interest.

Appendix A. Parametric Values of Hybrid PS [8,23,48]

Parameters and Their Values for LFC Model			
Parameter	Value	Parameter	Value
R_t (Hz/MW)	2.4	Rg (Hz/MW)	2.4
R_h (Hz/MW)	2.4	Kps1, Kps2	68.97
Tps1, Tps2	11.49	β1, β2	0.4312
Parameters and their values for Reheat Thermal Power System			
K_{re}	0.3	T_{tr}	0.3
T_{re}	10	T_{gr}	0.08
K_t	0.54367		
Parameters and their values for Gas Power System			
X	0.6	T_{CR}	0.01
b	0.049	C	1
a	1	Y	1.1
K_g	0.8	T_{CD}	0.2
T_F	0.239		
Parameters and their values for Hydro Power System			
Tr	5	T_{rh}	28.749
T_w	1	T_{gh}	0.2
Kh	0.32586		
Parameters and their values for Renewable energy resources			
K_{WTG}	1	T_{WTG}	1.5
Ts	1	T_T	0.3
Ks	0.5	K_T	1
Parameters and their values for Boiler Dynamic			
T_{1b}	0.545	K1b	0.950
Trb	0.545	Tf	0.23
Cb	200	K3	0.92
K1	0.85	K2	0.095
Tr	1.4	T_{rh}	28.75

Appendix B. Value of JSO Parameters

Parameters	Values	Parameters	Values	Parameters	Values	Parameters	Values
No of Population (Np)	40	No of Iteration	80	Lower limit (Lb)	−2	Upper Limit (Ub)	2
No of dimension	5	Constant factor (c_0)	4	Coefficient factor (γ)	>0		

References

1. Hassan, A.; Aly, M.; Elmelegi, A.; Nasrat, L.; Watanabe, M.; Mohamed, E.A. Optimal Frequency Control of Multi-Area Hybrid Power System Using New Cascaded TID-PI$^{\lambda}$D$^{\mu}$N Controller Incorporating Electric Vehicles. *Fractal Fract.* **2022**, *6*, 548. [CrossRef]
2. Barakat, M. Novel chaos game optimization tuned-fractional-order PID fractional-order PI controller for load–frequency control of interconnected power systems. *Prot. Control Mod. Power Syst.* **2022**, *7*, 16. [CrossRef]
3. Daraz, A.; Malik, S.A.; Waseem, A.; Azar, A.T.; Haq, I.U.; Ullah, Z.; Aslam, S. Automatic generation control of multi-source interconnected power system using FOI-TD controller. *Energies* **2021**, *14*, 5867. [CrossRef]
4. Khamies, M.; Magdy, G.; Ebeed, M.; Kamel, S. A robust PID controller based on linear quadratic Gaussian approach for improving frequency stability of power systems considering renewables. *ISA Trans.* **2021**, *117*, 118–138. [CrossRef] [PubMed]
5. Debnat, M.K.; Patel, N.C.; Mallick, R.K. Optimal base PD-PID controller for automatic generation control of multi-source tuned by teaching learning base optimization algorithm. In Proceedings of the 7th International Conference on Power Electronics (IICPE), Patiala, India, 17–19 November 2016; pp. 1–6.
6. Guha, D.; Roy, P.K.; Banerjee, S. Disturbance observer aided optimised fractional-order three-degree-of-freedom tilt-integral-derivative controller for load frequency control of power systems. *IET Gener. Transm. Distrib.* **2021**, *15*, 716–736. [CrossRef]
7. Daraz, A.; Malik, S.A.; Haq, I.U.; Khan, K.B.; Laghari, G.F.; Zafar, F. Modified PID controller for automatic generation control of multisource interconnected power system using fitness dependent optimizer algorithm. *PLoS ONE* **2020**, *15*, e0242428. [CrossRef]
8. Arya, Y.; Kumar, N. BFOA-scaled fractional order fuzzy PID controller applied to AGC of multi-area multi-source electric power generating systems. *Swarm Evol. Comput.* **2017**, *32*, 202–218. [CrossRef]

9. Fathy, A.; Kassem, A.M. Antlion optimizer-ANFIS load frequency control for multi-interconnected plants comprising photovoltaic and wind turbine. *ISA Trans.* **2019**, *87*, 282–296. [CrossRef]
10. Shah, R.; Preece, R.; Barnes, M. The impact of voltage regulation of multi-infeed VSC-HVDC on power system stability. *IEEE Trans. Energy Convers.* **2018**, *33*, 1614–1627. [CrossRef]
11. Zhang, G.; Mccalley, J.; Wang, Q. An AGC dynamics-constrained economic dispatch model. *IEEE Trans. Power Syst.* **2019**, *34*, 3931–3940. [CrossRef]
12. Gupta, A.K. Robust coordinated control for damping low frequency oscillations in high wind penetration power system. *Int. Trans. Electr. Energ Syst.* **2019**, *29*, e12006. [CrossRef]
13. Latif, A.; Hussain, S.M.S.; Das, D.C.; Ustun, T.S. State-of-the-art of controllers and soft computing techniques for regulated load frequency management of single/multi-area traditional and renewable energy-based power systems. *Appl. Energy* **2020**, *266*, 114858. [CrossRef]
14. Khezri, R.; Oshnoei, A.; Oshnoei, S.; Bevrani, H.; Muyeen, S.M. An intelligent coordinator design for GCSC and AGC in a two-area hybrid power system. *Appl. Soft Comput.* **2019**, *76*, 491–504. [CrossRef]
15. Ganguly, S.; Mahto, T.; Mukherjee, V. Integrated frequency and power control of an isolated hybrid power system considering scaling factor based fuzzy classical controller. *Swarm Evol. Comput.* **2017**, *32*, 184–201. [CrossRef]
16. Guha, D.; Roy, P.; Banerjee, S. Performance evolution of different controllers for frequency regulation of a hybrid energy power system employing chaotic crow search algorithm. *ISA Trans.* **2021**, *113*, 231–241. [CrossRef]
17. Latif, A.; Hussain, S.M.S.; Das, D.C.; Ustun, T.S. Double stage controller optimization for load requency stabilization in hybrid wind-ocean wave energy based maritime microgrid system. *Appl. Energy* **2021**, *282*, 116171. [CrossRef]
18. Prostejovsky, A.M.; Marinelli, M.; Rezkalla, M.; Syed, M.H.; Guillo-Sansano, E. Tuningless load frequency control through active engagement of distributed resources. *IEEE Trans. Power Syst.* **2018**, *33*, 2929–2939. [CrossRef]
19. Irudayaraj, A.X.R.; Wahab, N.I.A.; Umamaheswari, M.; Radzi, M.A.M.; Sulaiman, N.B.; Veerasamy, V.; Prasanna, S.C.; Ramachandran, R. A Matignon's theorem-based stability analysis of hybrid power system for automatic load frequency control using atom search optimized FOPID controller. *IEEE Access* **2020**, *8*, 168751–168772. [CrossRef]
20. Ahmed, M.; Magdy, G.; Khamies, M.; Kamel, S. Modified TID controller for load frequency control of a two-area interconnected diverse unit power system. *Int. J. Electr. Power Energy Syst.* **2022**, *135*, 107528. [CrossRef]
21. Bhuyan, M.; Das, D.C.; Barik, A.K. Proficient power control strategy for combined solar gas turbine-wind turbine generator-biodiesel generator based two area interconnected microgrid employed with DC link using Harris's hawk optimization optimised tilt-integral-derivative controller. *Int. J. Numer. Model. Electron. Netw. Device Fields* **2022**, *35*, e2991. [CrossRef]
22. Khamari, D.; Sahu, R.K.; Gorripotu, T.S.; Panda, S. Automatic generation control of power system in deregulated environment using hybrid TLBO and pattern search technique. *Ain Shams Eng. J.* **2019**, *11*, 553–573. [CrossRef]
23. Daraz, A.; Abdullah, S.; Mokhlis, H.; Haq, I.U.; Fareed, G.; Mansor, N.N. Fitness dependent optimizer-based automatic generation control of multisource interconnected power system with non-linearities. *IEEE Access* **2020**, *8*, 100989–101003. [CrossRef]
24. Yousri, D.; Babu, T.S.; Fathy, A. Recent methodology-based Harris hawks optimizer for designing load frequency control incorporated in multi-interconnected renewable energy plants. *Sustain. Energy Grids Netw.* **2020**, *22*, 100352. [CrossRef]
25. Kalyan, C.N.S.; Rao, G.S. Coordinated SMES and TCSC damping controller for load frequency control of multi area power system with diverse sources. *Int. J. Electr. Eng. Inform.* **2020**, *12*, 747–769. [CrossRef]
26. Priyadarshani, S.K.R.; Subhashini; Satapathy, J.K. Path finder algorithm optimized fractional order tilt-integral-derivative (fotid) controller for automatic generation control of multi-source power system. *Microsyst. Technol.* **2020**, *27*, 23–35. [CrossRef]
27. Arya, Y. Effect of electric vehicles on load frequency control in interconnected thermal and hydrothermal power systems utilising CFFOIDF controller. *IET Gener. Transm. Distrib.* **2020**, *14*, 2666–2675. [CrossRef]
28. Lal, D.K.; Barisal, A.K. Grasshopper algorithm optimized fractional order fuzzy PID frequency controller for hybrid power systems. *Recent Adv. Electr. Electron. Eng.* **2019**, *12*, 519–531. [CrossRef]
29. Hasanien, H.M.; El-Fergany, A.A. Salp swarm algorithm-based optimal load frequency control of hybrid renewable powersystems with communication delay and excitation cross-coupling effect. *Electr. Power Syst. Res.* **2019**, *176*, 105938. [CrossRef]
30. Ali, M.; Kotb, H.; Aboras, K.M.; Abbasy, N.H. Design of Cascaded PI-Fractional Order PID Controller for Improving the Frequency Response of Hybrid Microgrid System Using Gorilla Troops Optimizer. *IEEE Access* **2021**, *9*, 150715–150732. [CrossRef]
31. Nayak, N.; Mishra, S.; Sharma, D.; Sahu, B.K. Application of modified sine cosine algorithm to optimally design PID/fuzzy-PID controllers to deal with AGC issues in deregulated power system. *IET Gener. Transm. Distrib.* **2019**, *13*, 2474–2487. [CrossRef]
32. Lal, D.K.; Barisal, A.; Tripathy, M. Grey wolf optimizer algorithm based fuzzy PID controller for AGC of multi-area power system with TCPS. *Procedia Comput. Sci.* **2016**, *92*, 99–105. [CrossRef]
33. Jagatheesan, K.; Anand, B.; Samanta, S.; Dey, N.; Santhi, V.; Ashour, A.S.; Balas, V.E. Application of flower pollination algorithm in load frequency control of multi-area interconnected power system with nonlinearity. *Neural Comput. Appl.* **2016**, *28*, 475–488. [CrossRef]
34. Yakout, A.H.; Sabry, W.; Abdelaziz, A.Y.; Hasanien, H.M.; AboRas, K.M.; Kotb, H. Enhancement of frequency stability of power systems integrated with wind energy using marine predator algorithm based PIDA controlled STATCOM. *Alex. Eng. J.* **2022**, *61*, 5851–5867. [CrossRef]
35. Elkasem, A.H.A.; Khamies, M.; Hassan, M.H.; Agwa, A.M.; Kamel, S. Optimal Design of TD-TI Controller for LFC Considering Renewables Penetration by an Improved Chaos Game Optimizer. *Fractal Fract.* **2022**, *6*, 220. [CrossRef]

36. Kumari, S.; Shankar, G. Novel application of integral-tilt-derivative controller for performance evaluation of load frequency control of interconnected power system. *IET Gener. Transm. Distrib.* **2018**, *12*, 3550–3560. [CrossRef]
37. Chou, J.S.; Molla, A. Recent advances in use of bio-inspired jellyfish search algorithm for solving optimization problems. *Sci. Rep.* **2022**, *12*, 19157. [CrossRef]
38. Chou, J.-S.; Truong, D.-N.; Le, T.-L.; Truong, T.T.H. Bio-inspired optimization of weighted-feature machine learning for strength property prediction of fiber-reinforced soil. *Expert Syst. Appl.* **2021**, *180*, 115042. [CrossRef]
39. Ginidi, A.; Elsayed, A.; Shaheen, A.; Elattar, E.; El-Sehiemy, R. An innovative hybrid heap-based and jellyfish search algorithm for combined heat and power economic dispatch in electrical grids. *Mathematics* **2021**, *9*, 2053. [CrossRef]
40. Chou, J.S.; Tjandrakusuma, S.; Liu, C.Y. Jellyfish search-optimized deep learning for compressive strength prediction in images of ready-mixed concrete. *Comput. Intell. Neurosci.* **2022**, *2022*, 9541115. [CrossRef]
41. Daraz, A.; Malik, S.A.; Azar, A.T.; Aslam, S.; Alkhalifah, T.; Alturise, F. Optimized Fractional Order Integral-Tilt Derivative Controller for Frequency Regulation of Interconnected Diverse Renewable Energy Resources. *IEEE Access* **2022**, *10*, 43514–43527. [CrossRef]
42. Arya, Y. A new optimized fuzzy FOPI-FOPD controller for automatic generation control of electric power systems. *J. Frankl. Inst.* **2019**, *356*, 5611–5629. [CrossRef]
43. Sahu, R.; Gorripotu, T.; Panda, S. A hybrid DE-PS algorithm for load frequency control under deregulated power system with UPFC and RFB. *Ain Shams Eng. J.* **2015**, *6*, 893–911. [CrossRef]
44. Daraz, A.; Malik, S.A.; Mokhlis, H.; Haq, I.U.; Zafar, F.; Mansor, N.N. Improved-fitness dependent optimizer based foi-pd controller for automatic generation control of multi-source interconnected power system in deregulated environment. *IEEE Access* **2020**, *8*, 197757–197775. [CrossRef]
45. Ali, T.; Malik, S.A.; Daraz, A.; Aslam, S.; Alkhalifah, T. Dandelion Optimizer-Based Combined Automatic Voltage Regulation and Load Frequency Control in a Multi-Area, Multi-Source Interconnected Power System with Nonlinearities. *Energies* **2022**, *15*, 8499. [CrossRef]
46. Khamies, M.; Magdy, G.; Hussein, M.E.; Banakhr, F.A.; Kamel, S. An Efficient Control Strategy for Enhancing Frequency Stability of Multi-Area Power System Considering High Wind Energy Penetration. *IEEE Access* **2020**, *8*, 140062–140078. [CrossRef]
47. Tasnin, W.; Saikia, L.C.; Raju, M. Deregulated AGC of multi-area system incorporating dish-Stirling solar thermal and geothermalpower plants using fractional order cascade controller. *Int. J. Electr. Power Energy Syst.* **2018**, *101*, 60–74. [CrossRef]
48. Mohamed, E.A.; Ahmed, E.M.; Elmelegi, A.; Aly, M.; Elbaksawi, O.; Mohamed, A.-A.A. An optimized hybrid fractional order controller for frequency regulation in multi-area power systems. *IEEE Access* **2020**, *8*, 213899–213915. [CrossRef]
49. Elmelegi, A.; Mohamed, E.A.; Aly, M.; Ahmed, E.M.; Mohamed, A.-A.; Elbaksawi, O. Optimized tilt fractional order cooperative controllers for preserving frequency stability in renewable energy-based power systems. *IEEE Access* **2021**, *9*, 8261–8277. [CrossRef]